LATERAL INTERACTIONS AMONG MEMBRANE PROTEINS

Implications for the Organization of Gap Junctions

JAMES R. ABNEY, JOCHEN BRAUN, AND JOHN C. OWICKI
Department of Biophysics and Medical Physics, University of California, Berkeley, and Division of Biology and Medicine, Lawrence Berkeley Laboratory, University of California, Berkeley, California 94720

ABSTRACT We have studied the relationship between interprotein forces and the lateral distribution of proteins in disordered mouse liver gap junctions. Data on protein positions are obtained from freeze-fracture electron micrographs. Short-ranged correlations in observed positions are characteristic of interacting particles in a fluid state. An analysis derived from statistical mechanics allows the determination of the magnitude and functional form of interprotein forces. We find that jap junction proteins are mutually repulsive, in a manner consistent with electrostatics and excluded volume. This dictates that long-ranged protein aggregation into jap junction plaques cannot arise solely from interparticle interactions. An alternative is the balance of lateral pressures between the junction and the surrounding glycocalyx. This idea is quantified into a model. Junctional pressure arises from protein–protein interactions and is computed from a pressure equation based on the force and a radial distribution function describing order. The pressure from the glycocalyx is assumed to arise from mixing, electrostatic, and elastic interactions of sugar residues, and is described with terms from Flory–Krigbaum and McMillan–Mayer theories. The results of this modeling are in reasonable agreement with available experimental data.

1. INTRODUCTION

Gap junctions are specialized membrane protein assemblies thought to mediate direct cell-to-cell communication. They are aggregates of identical protein channels, called dyads, that bridge the intercellular space. The morphology of these aggregates—size, shape, and dyad packing order—varies with tissue. In liver, several thousand dyads form a plaque with a distinct boundary. Glycosylated membrane components are excluded from the plaque (Gilula, 1974; Hertzberg and Gilula, 1979; Gros et al., 1982) but are an integral part of a carbohydrate matrix, called the glycocalyx, that occupies the extra-junctional intercellular space. Current understanding of the structure and function of jap junctions has been extensively reviewed; pertinent discussions include Loewenstein (1981), Larsen (1983), De Mello (1984), Peracchia (1985), and Bennett and Spray (1985).

Forces between dyads and the mechanisms underlying the development and architecture of gap junctions are not well understood. We contend that both formation and morphology may follow largely or wholly from rather nonspecific physical properties of mobile, interacting dyads and the involved membranes. It is generally established that junctions assemble by the aggregation of precursors (both single dyads and small patches) already present but scattered in the membrane (Johnson et al., 1974; Yee and Revel, 1978; Tadvalkar and Pinto da Silva, 1983; Ryerse et al., 1984; Shivers and Bowman, 1985). Similarly, junctional regression may involve a redispersal of split junctional proteins, or connexons, over the membrane (Lane and Swales, 1980; Preus et al., 1981). Thus, both processes appear to require proteins that are laterally mobile.

Formation of gap junctions occurs spontaneously upon close apposition of neighboring membranes. In experiments on early amphibian embryos, junctions were shown to form between cells at arbitrary points of contact (Ito et al., 1974). In some tissues, so-called "reflexive" junctions have been reported connecting different regions of the same cell (reviewed briefly by Larsen, 1983); they may or may not be inappropriately formed. Both points suggest that cells may not select the site of junction formation, but that it is determined fundamentally by membrane interactions.[1]

What causes the dyads to be aggregated into plaques?

J. Braun's present address is Department of Applied Mathematics and Computer Science, Weizmann Institute for Science, Rehovot, 76100 Israel.
Address correspondence to J. C. Owicki.

[1]Junction formation that consistently occurs at specific regions of the cell (e.g., the lateral surfaces of polarized endothelial cells) could reflect an already close apposition of cell surfaces in these areas, a restriction of junctional precursors to the associated domains (Gumbiner and Louvard, 1985), or some other physiological mechanism.

Research suggests that junctional morphology is determined without attachment of dyads to an underlying cytoskeleton in mouse liver (Hirokawa and Heuser, 1982) and other tissues (e.g., Peracchia and Peracchia, 1980; Tadvalkar and Pinto da Silva, 1983). This does not preclude cytoskeletal involvement at other stages in junction development (e.g., Rassat et al., 1981, 1982; Tadvalkar and Pinto da Silva, 1983; Green and Severs, 1984). Evidence from chemical characterizations, diffraction, and most electron microscopy (e.g., Caspar et al., 1977; Makowski et al., 1977; Hirokawa and Heuser, 1982; Zampighi and Simon, 1985) suggests the absence of direct protein cross-links between dyads. One study based on electron crystallography observed an enhanced electron density between dyads that, it was noted, could represent unfolded portions of the dyad protein (Wrigley et al., 1984). The only published evidence for direct bridges, based on electron micrographs from freeze-etched, rotary-shadowed specimens, is highly inferential (Peracchia and Peracchia, 1985). An earlier study using the same technique failed to resolve cross-links at all (Hirokawa and Heuser, 1982). Instead, the interactions between dyads probably reflect electrostatics, excluded volume (i.e., contact repulsions) and lipid-mediated forces.

In this work, we use a statistical–mechanical technique described in a companion paper (Braun et al., 1987; henceforth BAO) to determine the nature of the forces between dyads and the mechanisms underlying dyad aggregation. Our studies focus on an analysis of dyad positions revealed in freeze-fracture electron micrographs of fast-frozen gap functions from mouse liver (Raviola et al., 1980). We begin by considering how a fluid-theoretic approach can be used to quantify the short-range of dyads within the junction and to extract the forces acting between particles. For this system, dyads are found to be mutually repulsive at all separations. Possible origins of the inter-dyad force are next discussed in detail, together with a technique to separate pair forces from multibody forces. We conclude by showing how this short-range data on order and forces can be combined with other information to model dyad aggregation into plaques despite the energetic barrier created by dyad repulsions. Our approach is based on the balance across the boundary of the plaque of the lateral pressures arising within the junction and the surrounding glycocalyx. A preliminary report of some of our findings has appeared elsewhere (Braun et al., 1984).

2. MATERIALS AND METHODS

Freeze-fracture electron micrographs of gap junctions from mouse liver were obtained as a generous gift from E. Raviola and were part of a previous study published as Raviola et al. (1980). The tissue samples used were rapidly frozen from the living state using the technique of Heuser et al. (1979), which is thought to preserve the in vivo distribution of intramembrane particles (see BAO). Micrograph magnifications were obtained by setting the observed lateral density of dyads equal to 9,330/μm^2 (as in Fig. 13 of Raviola et al., 1980). These magnifications are probably accurate to within 10%, in both absolute and relative (i.e., micrograph to micrograph) terms. Fig. 1 shows a micrograph representative of those used.

Our study used quantitative information on dyad positions that required computer manipulation. To facilitate data acquisition into the computer, portions of original micrographs were photographed and enlarged to a particle density of ~20 per square inch. Prints were then affixed to a 4953 graphics tablet (Tektronix, Inc., Beaverton, OR), which has an active area of 10 × 10 in. and a resolution of 100 lines/in. A convex polygonal area was staked out in the interior of the junctional plaque for analysis; borders of the plaque and more sparsely populated membrane areas outside it were identified visually and excluded from the area to be analyzed.

Coordinates of particles within the polygonal boundary were then entered manually by marking the apparent center of each particle with a magnetic pen. These data were stored in a computer file for further processing. Fig. 2 displays a computer-generated representation of one of the magnified regions. Such figures enabled us to compare the tabulated data with the original micrograph and to make corrections for misentered or missing particles. We estimate that >95% of the thousands of particles in the micrographs analyzed could be unambiguously identified; for the remaining particles that were either part of close aggregates and not clearly distinguishable or else incompletely preserved or shadowed, center positions were estimated heuristically. To this end, particles with coordinate separations of less than a specified distance were considered the same particle mistakenly entered twice and were replaced by a single set of coordinates at the average position. We estimate the fraction of particles overlooked and not entered to be <1%. These could be identified using plots such as Fig. 2 and their coordinates appended to the data file. However, the effects of one percent data omission were found to be small (data not shown) in studies on simulated electron micrographs such as those described in BAO.

Certain calculations were simplified by the choice of a hard core diameter, r_{HC}, for the junctional particles. Results of such computations were not sensitive to small variations in this quantity. For consistency with experimental results discussed in Section 4.1, we have chosen r_{HC} = 7.0 nm.

The radial distribution function, $g(r)$, and an angle-integrated triplet distribution function, $K(r,s)$, were computed using the particle coordinates according to the algorithms presented in the previous paper (BAO). The coordinate system used in these computations is shown in Fig. 3. The radial distribution function measures the probability of finding a second particle in the system a distance r from a given first one. The angle-integrated triplet distribution function is the number density of particles observed at polar coordinates (s, ϑ) with respect to a pair of particles separated by r, multiplied by $\cos(\vartheta)$, and integrated over ϑ. These functions were tabulated over bins of width Δ to reduce noise arising from the finite sample size.

The distribution functions initially displayed substantial artifacts due to the correlation of grid points on the square lattice of the digitization tablet. Further enlargement of the micrographs, or alternatively the use of a finer digitization grid, could have reduced this problem but was not feasible due to the limiting size and resolution of the available graphics tablet. We ultimately overcame these artifacts by adding a random number ranging from −0.5 to +0.5 grid units (−0.005 to +0.005 in.) to both x and y coordinates. The degradation of the data involved in this "coordinate smearing" was small, as determined using simulated electron micrographs (data not shown), and was minimized further by averaging the results of several different randomizations for each data set.

These distribution functions were used to calculate the effective pair force, $f(r)$, acting between dyads. This was done using the Born–Green–Yvon (BGY) equation

$$kT\frac{\mathrm{d}\ln g(r)}{\mathrm{d}r} = f(r) + \int_0^\infty f(s)K(r,s)\,\mathrm{d}s \qquad (1)$$

described previously (BAO). The left-hand side of this equation represents the statistical mean force acting on a particle at the origin, where kT

FIGURE 1 Freeze-fracture electron micrograph of a gap junction from mouse liver, denoted junction 1. The gap junction proteins (dyads) are seen to be aggregated into a plaque at a density of 9,330/μm^2 and an average center-to-center spacing of ~10.6 nm. Particles in the surrounding membranes, which may include glycosylated species, are much more disperse. Analysis of this junction proceeded on high-quality enlargements. Two or more such regions were analyzed for each junction, avoiding edges that introduce inhomogeneities.

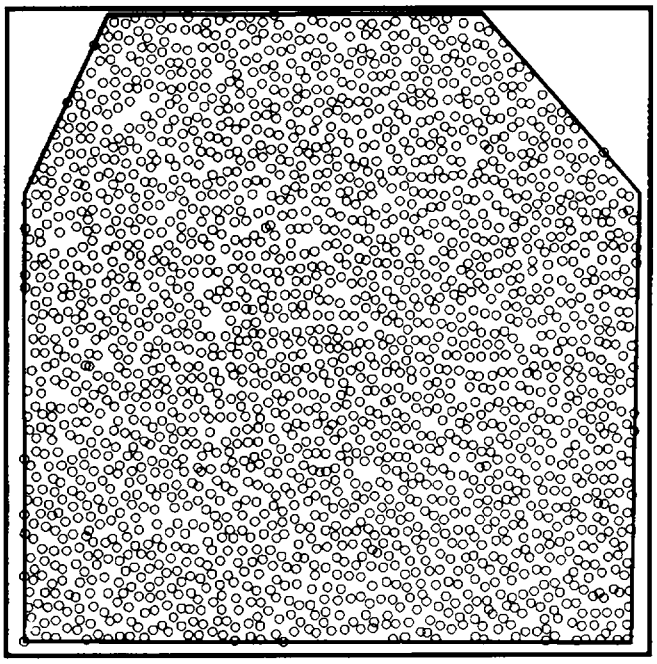

FIGURE 2 Computer representation of single enlarged region from junction 1, with coordinate system. The interior convex polygonal boundary indicates the edges of the region analyzed; the outer rectangular boundary indicates the extent of the digitization tablet. Particles have been drawn to a diameter of 7 nm as discussed in the text. This region has an area of 0.233 μm^2 and contains 2,189 particles. Overlapping and missing particles probably reflect errors in data entry; with these exceptions, particle positions are thought to be correct to within 0.5–1.0 nm. The effects of these errors are minor and are discussed more fully in the text.

is the thermal Boltzmann energy. The mean force arises from two sources: the direct interaction from the particle at r, $f(r)$, and the component along r of the interaction from all other particles, represented by the integral. The use of discrete distribution functions reduced the BGY equation to a system of linear equations with $f(r)$ as its solution. The number of equations is determined by the bin width and the lower and upper limits, r_{min} and r_{max}, imposed on the integral by numerical considerations. The number r_{min} represents the smallest interparticle separation observed, whereas r_{max} is chosen arbitrarily but is large enough to include all ordering in the distribution functions.

Derivatives were computed using a five-point cubic/quartic fit as described by Savitzky and Golay (1964). The pair force was integrated numerically to obtain the pair potential, $u(r) = -\int_{r_{max}}^{r} f(r')\,dr'$, using Simpson's rule (Bevington, 1969):

$$u(r_i) = \frac{3}{2}\Delta[f(r_i) + 4f(r_{i+1}) + 2f(r_{i+2}) + 4f(r_{i+3}) + \ldots] \quad (2)$$

Such an expression implictly sets $u(r) \equiv 0$ for $r > r_{max}$.

Using the computed pair potential, the radial distribution function appropriate to a fluid at the experimental density was obtained by Monte Carlo simulation using the algorithm of Metropolis et al. (1953). The computer program was the same one used in BAO; there were 256 particles with periodic boundary conditions. This method simulates the chosen fluid with great accuracy and with precision limited only by the amount of computer time spent to reduce stochastic noise in the results.

3. RESULTS

We present results from two junctions. The radial distribution function, $g(r)$, for the junction in Fig. 1 (henceforth

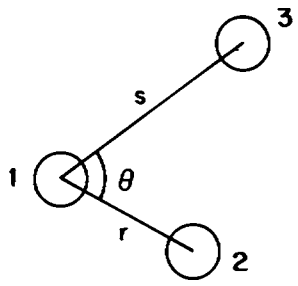

FIGURE 3 Coordinate system used in evaluation of distribution functions.

junction 1) is shown in Fig. 4. Its form is typical of radial distribution functions for simple fluids: a value near zero for small r (roughly indicating particle diameter), a prominent initial peak at larger r (indicating the separation of nearest neighbors), and a series of peaks that decay toward a value of one as r increases still further (corresponding to the decay of order in maintaining subsequent coordination shells around the central particle). The effective pair force $f(r)$ between dyads in junction 1 is shown in Fig. 5. It is repulsive at small separations and appears to decay to zero by 20 nm. No attractions are evident. Integration of this force gives the interdyad pair potential $u(r)$, also displayed in Fig. 5.

The distribution functions from junction 2 showed weaker correlations than those from junction 1. The associated radial distribution function is shown in Fig. 6. The first peak is broader and of lower amplitude than its counterpart in Fig. 4. A second peak may also be seen, but additional features are difficult to distinguish from the noise. The force and potential determined for junction 2 are shown in Fig. 7. Despite the differences in $g(r)$, they are similar to, though weaker than, those shown in Fig. 5.

The radial distribution function obtained by the Monte Carlo simulation of the potential for junction 1 is displayed

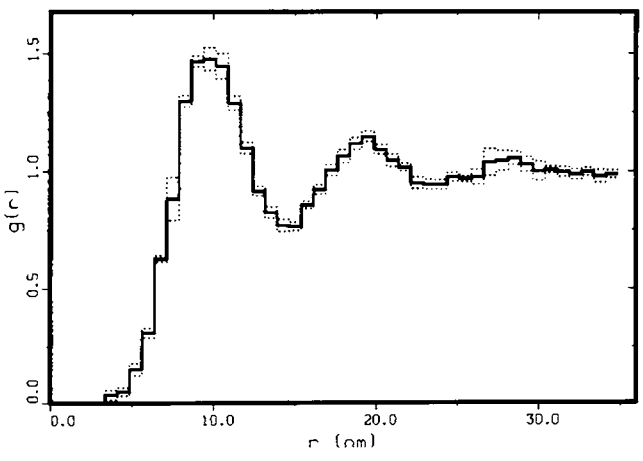

FIGURE 4 Radial distribution function, $g(r)$, for dyads within junction 1. The dotted error envelope represents the standard deviation obtained by separate analysis of the two regions in Fig. 1. Among other things, the tight distribution of errors suggests the uniformity and agreement of data compiled from various regions of the same junction. The calculation was performed over 47 bins of width 0.75 nm. A total of 4,317 particles were analyzed.

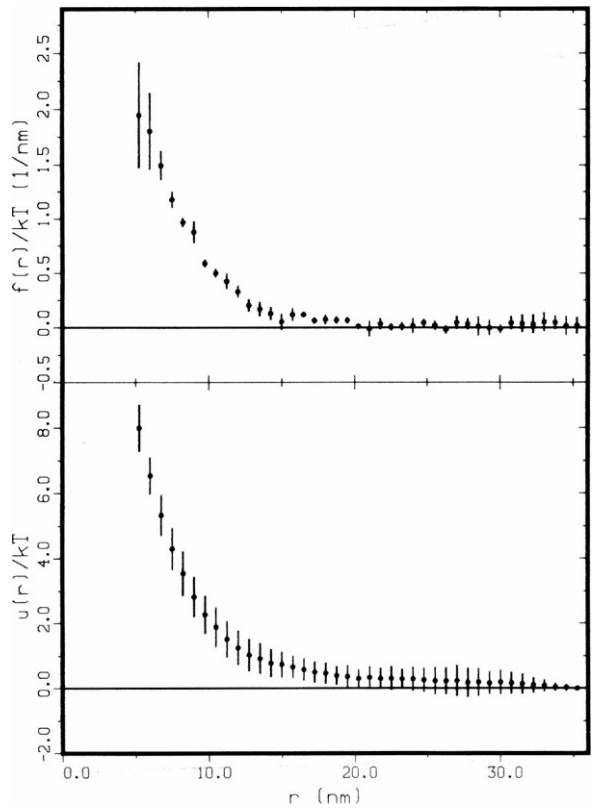

FIGURE 5 Effective pair force, $f(r)$, and potential, $u(r)$, for dyads within junction 1. The force was computed via the BGY equation; the potential computed by integrating (with Simpson's rule) the force over r. The potential represents the pair energy required to compress two dyads from a reference separation of 35 nm. If the force remains zero over the unanalyzed region this potential is equivalent to that obtained from a more standard infinite reference separation. Both the force and potential have been divided by the thermal Boltzmann energy, kT, where $T \approx 310$ K. The choice of bin width, the number of particles analyzed, and the computation of error bars are as described in Fig. 4.

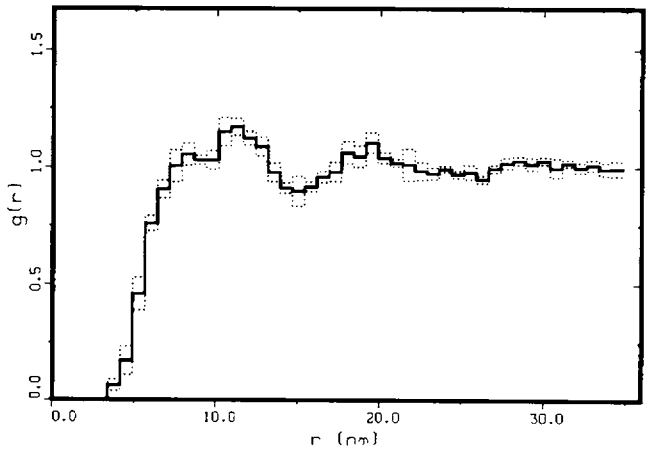

FIGURE 6 Radial distribution function for dyads within junction 2. As for junction 1 (Figs. 1, 2, 4, and 5), two nonoverlapping regions were analyzed. 47 bins 0.75-nm wide were again used in the analysis of 3,434 particles.

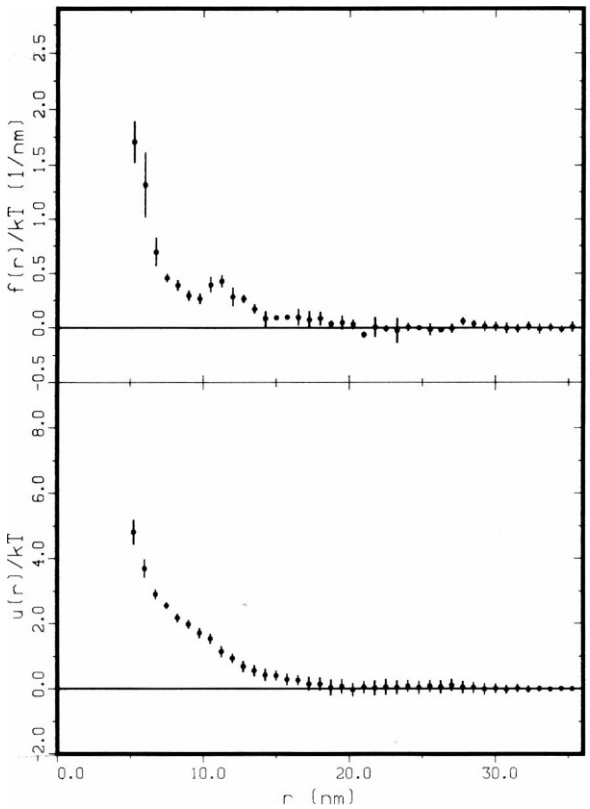

FIGURE 7 Effective pair force and potential for dyads within junction 2. The kink in the pair force near 10 nm is a reflection of the dip in bin occupancy at this separation displayed in Fig. 6. This could be a statistical fluctuation due to the finite sample size, or may indicate some unknown phenomenology. Despite the kink, the force and potential for junction 2 demonstrate the same functional form and range as their counterparts in junction 1. A more complete discussion appears in the text.

in Fig. 8, together with the empirical $g(r)$ for that junction. The agreement is quite good: the horizontal (r) positions of peaks and troughs are virtually identical, and the vertical scale is similar. The simulated $g(r)$ shows slightly weaker structure than the experimental $g(r)$.

4. DISCUSSION OF COMPUTED FORCES

The forces calculated between dyads include the effects of direct dyad–dyad interactions (e.g., electrostatic and excluded volume), as well as indirect, possibly multibody interactions (e.g., lipid-mediated) in an averaged way. These many contributions and the lack of detailed knowledge of dyad structure make a precise, quantitative understanding of the origin of the force impossible. Our studies emphasize instead the more complete picture of our system that can be derived once the force is known, independent of its precise origin (see, for example, the calculation of the lateral pressure in Section 5.1A). Nevertheless, there is merit in some discussion of the various contributions to the force and their relative roles: a reasonable understanding of the microscopic interactions within the system can be obtained from quite qualitative aspects of the computed force. In the rest of this section, we consider (a) a

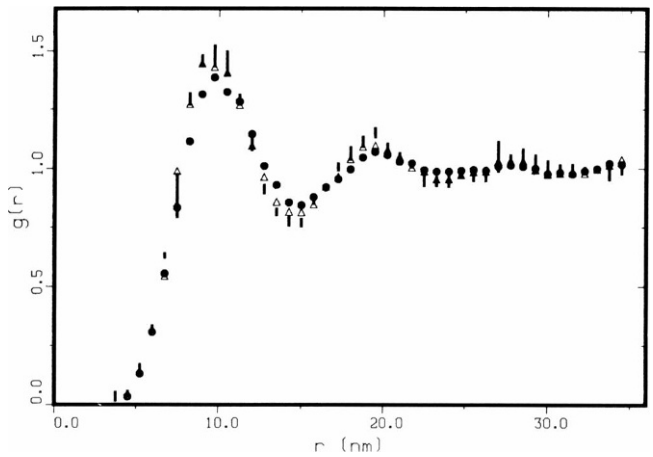

FIGURE 8 Radial distribution function from Monte-Carlo simulation of particle positions using potential derived from junction 1. The empirical $g(r)$ is represented together with error as a set of vertical bars. Simulation results (●) for r_{HC} = 4.9 nm, and (Δ) for r_{HC} = 7.0 nm. The error in the Monte-Carlo results is estimated at 2–5% (BAO).

description of the forces calculated for the two junctions analyzed; (*b*) mechanisms of dyad–dyad interaction, and their likely importance; and (*c*) a technique for possibly separating pair forces from three- and higher-body interactions.

4.1. Description of the Computed Forces

As noted in Results, dyads within both junctions display repulsive pair potentials that decay to zero without a trace of attractions. To be more quantitative, we compare range and magnitude with thermal energies that act to randomize particle positions. The pair potential allows a convenient way to make this comparison. Figs. 5 and 7 indicate that the interdyad potential becomes significant for both junctions relative to thermal particle energies (i.e., $u(r)/kT \approx 1$) near 12 nm, a distance greater than the average center-to-center particle separation in the system. That particle interactions are significant to at least this separation is qualitatively clear from the ordering in the system visible in the distribution functions (Figs. 4 and 6), but the force and potential are necessary for quantitative information.

We can also assess the small differences between the forces in the two junctions. It is possible that the interactions are more nearly identical, and that the observed difference is partially an artifact of our procedure for scaling magnifications to achieve the same particle density. The lower structure visible in junction 2 is characteristic of a system interacting at a lower density, where particles have less influence on their neighbors. If the particles in junction 2 were really at a lower density than those in junction 1, then our scaling effectively compressed the partiles in junction 2. Under such a compression, bin-by-bin values of dimensionless quantities such as $g(r)$ and $u(r)/kT$ do not change, but the value of r associated with each bin is decreased. The quantitative effect is straightforward: a 10% overestimate of the magnification would have decreased r by 10%. So, for example, what is reported as $u(9\text{ nm})/kT$ for junction 2 would really be $u(10\text{ nm})/kT$: the apparent physical extent of the interaction potential would have been reduced by the compression. A misestimate of this magnitude is sufficient to bring results from the two junctions into agreement. Such differences in lateral density among different plaques could reflect physiological variations in the mechanisms responsible for aggregating the dyads into plaques (see section entitled Modeling).

It is unlikely that dyads ever approach one another more closely than approximately 7 nm, based on the size of the proteins that can be estimated from lattice constants in crystalline plaques (e.g., Caspar et al., 1977; Makowski et al., 1977) and from reconstructions of scattering density using electron microscopy (Unwin and Zampighi, 1980). Nevertheless, we have observed separations down to 5.5 nm and have computed potentials of $\approx 8\ kT$ there. We underestimate the strong repulsions at protein–protein contact because of noise in the assignment of particle coordinates. Such noise slightly broadens the correlation functions, with significant impact primarily on regions where the functions are sharply varying; in other words, the initial rise of $g(r)$. The broadening extends the measured correlation function down to physically inaccessible regions, making them appear accessible with difficulty.

The broadening represents the convolution of some smearing function and the true distribution functions. If one could estimate the functional form (e.g., Gaussian, rectangular) and width of the smearing function, it should be possible to use Fourier deconvolution methods to recover the pristine correlation functions. We have not yet attempted this.

4.2. Origins of the Computed Forces

The role of possible contributions to the interdyad force will be assessed independently and in increasing order of their probable importance. Lipid-mediated protein/protein interactions have been predicted by theories of lipid–protein interactions (reviewed by Abney and Owicki, 1985). These arise due to protein-induced perturbations in lipid order and can display attractive or repulsive components. However we do not expect them to be dominant in the interdyad force. In most predictions, their range is smaller than that observed in the gap junction, and even near contact they only produce pair energies of approximately 1 kT. Even if their range is longer, in concentrated protein solutions such as the gap junction, perturbations of lipid order may be saturated (Pearson et al., 1984; Abney and Owicki, 1985). If variations in protein position have little affect on the lipid, a lipid-mediated force will be much diminished. Such saturation is not likely to pertain to the edges of the plaque (outside the region of our direct

analysis), and it is possible that longer-ranged lipid-mediated forces play some role in junctional cohesiveness, if not internal structure.

It is more likely that the interdyad force reflects simple volume exclusion for small separations and electrostatic repulsions at larger distances. Volume exclusion would imply strong repulsions at contact separations. Equal charges on the identical dyads would engender a repulsive force beyond this that decays to zero at sufficiently large distances. A quantitative assessment will require information on the number, location, and environment of charges, which is not yet available.

We can make some general statements concerning the effects of charge location and environment. Assuming the dyad is traversed by a single pore (e.g., for mouse liver Caspar et al., 1977; Makowski et al., 1977; for rat liver Unwin and Zampighi, 1980), charge must be located peripheral to the dyad axis. These charges could be located anywhere along the length of the dyad, from the ctyoplasm through the membrane and into the extracellular space. Symmetries in dyad structure (such as the established hexagonal rotational symmetry; see references immediately above) will give rise to symmetries in charge location.

The form of the electrostatic interaction is determined by environment. In an electrolytic medium, such as the cytoplasm or extracellular space, interactions follow the Debye–Huckel form, $(\kappa + 1)r^{-1} \exp(-\kappa r)$ (Lewis and Randall, 1961). Here $1/\kappa$ is a decay length constant that depends on ionic strength. Charges buried in the membrane interact to good approximation according to a force law proportional to r^{-4} (Tsien, 1978; Tsien and Hladky, 1982).

Thus, the net electrostatic interaction between dyads may be a very complicated function when referred to the center-to-center separation of the proteins. It will depend on the pair-wise interactions of charges whose separations may deviate substantially from the center-to-center separation. Moreover, the pair-wise forces typically do not act precisely along the vector between dyad centers and thus must be resolved. Finally, the pair-wise interactions are modified by whatever medium (media) intervene.

4.3. Separation into Pair and Higher-Body Forces

As was discussed in BAO, our BGY analysis assumes that the potential U governing N dyads is pair-wise additive, i.e.,

$$U(\mathbf{r}_1, \mathbf{r}_2 \ldots \mathbf{r}_N) = \sum_{1=i<j}^{N} u(r_{ij}). \tag{3}$$

There may well exist contributions to U that intrinsically involve the coordinates of triplets or larger groupings of particles. If so, the potential that we have determined will include these higher-body interactions in some averaged way. A fluid governed by the pair-wise additive potential that we have determined will then, in general, have different properties (e.g., $g(r)$) from the experimental system that we used to obtain the potential.

A self-consistency check for pair-wise additivity can be performed by comparing the experimental $g(r)$ with one obtained by simulating a fluid governed by the computed pair potential. The results of such a Monte Carlo simulation are shown in Fig. 8. The good agreement demonstrates that multibody forces do not contribute very much to positional correlations in these junctional plaques at the observed particle densities.

The slightly weaker oscillations in the simulated compared with the experimental $g(r)$ may reflect minor effects of multibody forces. Alternatively, they may be caused by noise in the assignment of particle coordinates, as discussed in Section 4.1. Such noise, which does not reflect pair-wise additive interactions, causes broadening of correlation functions and softening of derived pair potentials. We note in this regard that increasing the hard-core diameter to 7.0 nm in the simulation brings the two $g(r)$ into substantial agreement for $r > r_{HC}$ (see Fig. 8).

Our results do not rule out the presence of substantial multibody forces in gap junctions. As discussed above, long-ranged multibody forces might saturate at the experimental particle densities. Thus we can claim that the interdyad forces that we have analyzed are apparently pair-wise additive under the observed conditions, but not necessarily truly pair-wise additive in the sense that one pair potential characterizes the system at all densities.

5. MODELING

Our concept of the processes involved in the formation and maintenance of gap junctions is displayed in Fig. 9. In the absence of membrane–membrane attachment, connexons and elements of the glycocalyx mix in the membranes (A). With the fusion of subunits to form dyads, apposing regions of membrane are pulled together (B). This process is accompanied by strong repulsions between components of the glycocalyx, since the separation of the membranes is substantially smaller than the thickness of the glycocalyx. These repulsions can be greatly reduced by a lateral phase separation that leads to the coalescence of the dyads to form the junction and the removal of glycolipids and glycoproteins from the compressed region (C). This is a development of a model we proposed earlier (Braun et al., 1984). In this section, we focus on the processes involved in determining the density of dyads in gap junctions, as in C.

Within the coalesced junction, repulsive interdyad forces create a lateral pressure Π_j that tends to minimize encounters between dyads by enlarging the junction. This pressure is offset by an external pressure Π_{ej} arising from interactions within the glycocalyx, a balancing role first proposed by Peracchia (1985). The equilibrium size of the

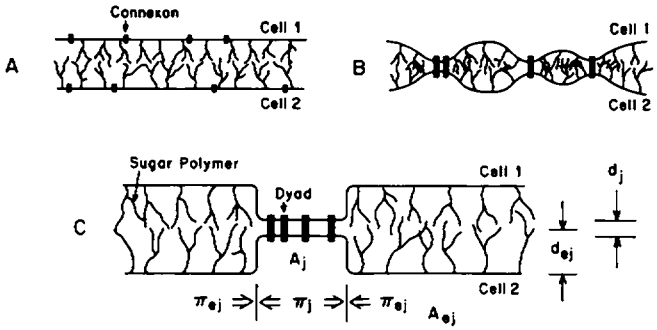

FIGURE 9 Schematic of model diagramming formation and equilibrium structure of a gap junction. *A* portrays two unlinked cells. Connexons and the membrane tethers of the glycocalyx intermix. In *B*, dyad formation has occurred by fusion of connexons through incompletely understood mechanisms. Adjacent regions of membrane are pulled close together, sterically excluding elements of the glycocalyx. *C* shows the junction at (dynamic) equilibrium. Energetic factors discussed under Modeling have led to the aggregation of dyads in the plaque. Bending near the edges of the plaque has been exaggerated to more clearly delineate the junctional and extra-junctional regions. Π_j and Π_{ej} refer to lateral pressure from elements of the junctional and extra-junctional space, respectively. Similarly, A_j and A_{ej} refer to areas involved in junctional and extra-junctional membrane. Finally, d_j denotes the membrane–membrane separation in the junction; d_{ej} denotes the extent of the glycocalyx surrounding each cell.

aggregate is determined by the Laplace equation (Adamson, 1982).

$$\Pi_j - \Pi_{ej} = f(\tau, c), \tag{4}$$

which states that the two pressures are equal to within some function, $f(\tau, c)$, of the tension (τ) and curvature (c) of the boundary separating the two domains.

To understand the origins and magnitude of the pressures and edge effects, we have modeled the system as two communicating compartments, representing the junctional and extra-junctional regions of the extracellular space. These are separated by an "edge" of curved membrane. Dyads and elements of the glycocalyx are confined to their respective compartments, while other species, such as charged and uncharged lipids within the membrane, and water and ions within solution, are freely exchanged.

The pressure from within each compartment can be calculated independently from interactions between its resident (nonexchanging) elements. The exchanging species are then considered unobserved degrees of freedom, and exert their influence by collectively constituting a "solvent" that can, for example, screen nonexchanging charges. Due to the exclusion of glycosylated residues (see earlier references), dyads are the only nonexchanging component of the junction. This suggests that the junctional pressure can be computed from the forces between dyads, as well as direct membrane–membrane interactions. The dyad–dyad contribution can be determined from our experimental data on the junctions analyzed, though membrane–membrane interactions must be treated empirically.

On the other hand, the extra-junctional pressure must reflect the various interactions that can take place among the many species confined to the extra-junctional space. Fortunately, some simplifications are possible. Protein–protein interactions, such as those considered between dyads within the junction, are probably small due to the lower protein density in the extra-junctional membrane and the presence of the glycocalyx, which may act to hold proteins apart. The order-of-magnitude larger separation of the membranes in the extra-junctional space likewise diminishes the role of direct membrane–membrane interactions. Therefore the predominant contributions to the extra-junctional lateral pressure probably come from interactions between sugar residues. These were not experimentally accessible but have been treated with a model that emphasizes mixing energies, electrostatic interactions, and conformational deformation within the glycocalyx. We have assumed that the pressure in each compartment can arise from several independent sources, with the total pressure given by their sum.

We are justified in neglecting boundary effects in applying the Laplace equation to this model. Gap-junctional plaques in mouse liver show marked deviations from circularity, with perimeters up to about twice those of circles of equivalent area; see, for example, Fig. 1. These deviations can be considered to be thermally excited capillary waves in the boundary of the plaque (Croxton, 1980). The amplitude of such waves involves the ratio of boundary energies to thermal energies. Variations in perimeter as large as those observed imply that boundary effects must be rather weak. This analysis is supported by more detailed modeling of the edge tension in terms of protein–protein interactions at the boundary and bending elasticity of the membrane normal to the plane of the junction (unpublished results). Given that other components of lateral pressures are found to be significantly stronger than ideal (thermal) lateral pressures, we set $f(\tau, c) = 0$ in Eq. 4 and take the equality of the junctional and extra-junctional lateral pressures as the condition of equilibrium. Edge effects will vary in importance inversely with the size of the junction, and they may contribute significantly to the equilibrium density in plaques smaller than those that we are analyzing.

Finally, our model emphasizes the factors involved in the determination of dyad density within the large gap junctions we analyzed in mouse liver and not junctional size. It may be that large plaques are ultimately favored to minimize the edge tension discussed above. However, the distribution of plaque sizes in a real cell might be determined kinetically by the relative rates of the internalization of membrane proteins and the coalescence of slowly diffusing plaques that originated from different nucleation events. Such processes are outside the scope of our model. The intermolecular interactions we consider should be insensitive to these kinetic factors and can be treated as equilibrated.

5.1. The Junctional Pressure

We model the junction as two closely apposed membranes with area A_j (Fig. 9). The dyads bridge this space and hold intermembrane separation constant at d_j. The dyads are thought to diffuse freely within the membranes, interacting according to the determined force. The lateral pressure exerted by the junction is assumed to arise from two sources: (A) direct dyad–dyad interactions, and (B) interactions between the two closely apposed membranes. We consider each in turn.

(A) Dyad–Dyad Interactions, $\Pi_{j,dd}$. Interactions between proteins contribute to the lateral pressure in a way that can be quantified using the pressure equation (BAO). It was shown in BAO that the interprotein force computed using the BGY technique reflects all interprotein interactions. In turn, the lateral pressures computed from the BGY force via the pressure equation also includes all contributions from interprotein interactions. For gap junctions, the pressure equation resolves the lateral pressure arising from interactions between dyads, $\Pi_{j,dd}$, into an ideal contribution reflecting particle translational energy and a nonideal contribution reflecting interactions between particles. The latter term weighs the force between particles at a specified separation by the number of particles possessing that separation, given in part by $g(r)$. The complete expression is

$$\frac{\Pi_{j,dd}}{kT} = \rho_d + \left(\frac{\rho_d^2}{4kT}\right)\int_0^\infty rf(r)g(r)2\pi r\, dr, \qquad (5)$$

where ρ_d is the number density of dyads. As the dyads are assumed to be the only nonexchanging molecules within the junction, they are the sole contributor to this two-dimensional osmotic pressure.

Eq. 5 is computationally straightforward and was evaluated in discrete form using Simpson's rule. The hard-core diameter manifested itself as a delta function in the force and had the effect of truncating the pressure integral below r_{HC}. This truncation was somewhat formal, since the pressure was not particularly sensitive to the precise choice of r_{HC}.

Using the data for junction 1, and a hard-core diameter of 7.0 nm, a value of $1.17(\pm 0.60) \times 10^{+13}\ kT/cm^2$ was derived for the pressure. The results from junction 2, with the same hard-core diameter, gave a slightly smaller lateral pressure of $0.67(\pm 0.23) \times 10^{+13}\ kT/cm^2$. In both cases the predominant contribution to the pressure came from the integral term of Eq. 5. The error estimates were obtained by averaging over nonoverlapping regions of the same junction, as in Figs. 4–7.

(B) Membrane–Membrane Interactions, $\Pi_{j,mm}$. The close apposition of adjacent cell membranes within the junction, ~2–3 nm (see review articles), suggests the possibility of direct membrane-membrane interactions. Charged lipids could lead to electrostatic double-layer repulsions. The exclusion of relatively ordered water begins near this separation to generate hydration forces. Finally, electrodynamic interactions could be manifested as van der Waals forces. For a brief review of membrane–membrane interactions with a biological emphasis, see Rand and Parsegian (1984); more detailed references are contained therein.

Membrane–membrane forces, by symmetry, act normal to the plane of the apposed membranes. However, they give rise to a lateral pressure because the total energy of interaction between the two membranes can be altered by changes in junctional area. We can express the combined effects of these interactions as a three-dimensional pressure, $p_{j,mm}$, that acts between membranes. To obtain the lateral pressure, we note $\Pi = p(\partial V/\partial A)_T$. If d_j is held constant, we obtain

$$\Pi_{j,mm} = -p_{j,mm}d_j. \qquad (6)$$

Unfortunately, without a detailed knowledge of the composition of the membranes, it is impossible to determine the form and magnitude of these interactions accurately. Lateral presures arising from electrostatic and van der Waals interactions are probably small compared with $\Pi_{j,dd}$ (unpublished results). We also neglect the effects of hydration forces, although for some lipid compositions and sufficiently close appositions, hydration forces could cause $\Pi_{j,mm}$ to be appreciable (Rand and Parsegian, 1984). We include $\Pi_{j,mm}$ in our analysis in only a formal sense, demonstrating that it can be consistent with junctional cohesion, but is not necessary to cause it.

5.2. Model for the Extra-junctional Pressure

We model the extra-junctional intercellular space as a uniform polymer coat of thickness $2d_{ej}$ and area A_{ej} (Fig. 9). For convenience the cell coats are shown touching, but separation does not affect any of the computed values. Segments within the polymer coat are sugar residues, which may carry charge and are assumed to interact with their neighbors and with the solvent. The constituent polymers are viewed as forming a single, interpenetrating matrix. This requirement of uniformity does not imply a smearing of the polymer segments or their charge to form a continuous system, but rather that the segments diffuse and so have an equal probability of occupying any position within the allowed volume V_{ej}.

We discuss in turn three contributions to the lateral pressure: (A) neutral mixing interactions between polymer and solvent, modeled with Flory–Krigbaum theory, (B) electrostatic repulsions between charged segments, modeled with McMillan–Mayer theory, and (C) conformational deformation of the matrix, which we consider to be small.

(A) Mixing, $\Pi_{ej,mx}$. Lateral compression of the glycocalyx leads to an increase in the density of polymer segments and a concomitant substitution of solvent–segment contacts for segment–segment contacts. This gives rise to a free energy of mixing that can be evaluated using Flory–Krigbaum theory (Flory and Krigbaum, 1950; Meier, 1967; Smitham et al., 1975; Napper, 1977; Bongrand and Bell, 1983).

Flory–Krigbaum theory describes mixing interactions between uncharged polymer chains, which are modeled as strings of like-sized, rigid segments. As suggested above, we make no distinction between individual polymer molecules, with the effects of compression thought to reside in the increased density of one large polymer network. By considering the free energies of solvent–solvent, solvent–segment, and segment–segment interactions, an expression is derived for the free energy of mixing of such a system relative to infinite dilution:

$$\Delta F_{ej,mx} = kT\left(\frac{V_s^2}{V_l}\right)\left(\frac{1}{2} - \chi\right)\left(\int_{V_{ej}} \rho_{ej}^2\, dV - \int_{V_{ej,\infty}} \rho_{ej,\infty}^2\, dV\right). \quad (7)$$

In this expression, V_s is the volume of a polymer segment, V_l is the volume of a solvent (water) molecule, χ is an empirical interaction parameter describing the favorability of solvent–segment interactions, and ρ_{ej} and $\rho_{ej,\infty}$ are density distribution functions for polymer segments at the observed concentration and infinite dilution, respectively.

We assume a uniform segment density that goes to zero for infinite dilution. Then

$$\Delta F_{ej,mx} = kT\left(\frac{V_s^2}{V_l}\right)\left(\frac{1}{2} - \chi\right)\rho_{ej}^2 V_{ej}. \quad (8)$$

In fact, Eq. 8 probably overestimates the energy since most glycoproteins contain multiple polymer chains that remain in contact even at infinite dilution. However, this does not affect the computed pressure, since the term reflecting the standard state is constant and hence vanishes upon differentiation.

The lateral pressure is obtained as for Eq. 6. We find

$$\frac{\Pi_{ej,mx}}{kT} = \left(\frac{V_s^2}{V_l}\right)\left(\frac{1}{2} - \chi\right)\rho_{ej}^2 2d_{ej} \quad (9)$$

where $\partial V_{ej}/\partial A_{ej} = 2d_{ej}$.

(B) Electrostatics, $\Pi_{ej,el}$. Lateral compression of the glycocalyx decreases the average separation between charged sugar residues and thus leads to an increase in repulsive electrostatic interactions. With the recognition that the glycocalyx represents a region of nonexchanging charge that can be likened to a Donnan equilibrium, the problem may be conveniently treated via McMillan–Mayer theory (Hill, 1956, 1960). We parallel a discussion in the latter reference, used there to describe the swelling of polyelectrolyte gels. We have modified that discussion to incorporate the presence of uncharged segments.

In the McMillan–Mayer approach, the Donnan contribution to the osmotic behavior is expressed as a virial expansion in ρ_{ej}, the three-dimensional number density of polymer segments:

$$\frac{p_{ej,el}}{kT} = \rho_{ej} + B_2(T)\rho_{ej}^2 + \ldots$$

$$= \rho_{ej} - \frac{(x\rho_{ej})^2}{2}\int_0^\infty [e^{-u(r)/kT} - 1]4\pi^2\, dr + \ldots \quad (10)$$

We only retain terms out to the second virial coefficient, $B_2(T)$. Here $u(r)$ gives the electrostatic interaction between two charged segments, while x denotes the fraction of segments bearing charge. The leading term is an ideal translational contribution for both charged and uncharged segments, $\rho_{ej} = x\rho_{ej} + (1 - x)\rho_{ej}$, while subsequent terms are nonzero only for interactions between charged segments. This virial expansion is fundamentally related to the exact pressure equation used in the calculation of the dyad–dyad pressure (Hill, 1960; McQuarrie, 1976). We use the virial expansion in this case because by a careful identification (see below) it can be evaluated using electroneutrality arguments, without explicit information on particle distribution or interparticle interactions.

Expansion of the exponential and retention of the first two terms considerably simplifies the integration in Eq. 10 and yields an approximate answer in simple closed-form. With the mild assumption of electroneutrality, we obtain

$$\frac{p_{ej,el}}{kT} = \rho_{ej} + \frac{x^2\rho_{ej}^2}{4N_A I_o}, \quad (11)$$

where N_A is Avogadro's number, and I_o is the ionic strength of the surrounding solution. In this approach we have evaluated the integral over the potential in Eq. 10 by assuming it arises indirectly from the excess of exchanging counterions necessary in the glycocalyx to screen the segment charge and preserve electroneutrality; it can be alternatively considered to reflect explicitly the repulsive electrostatic interactions between the like-charged segments (Hill, 1956).

Once again the polymer network is thought of as a single interpenetrating matrix: there is no segment contribution to the osmotic pressure. We therefore analyze Eq. 11 in the limit $\rho_{ej} \to 0$ while keeping the charge density, $x\rho_{ej}e$, constant. Here e is the charge on an electron. In this limit

$$\frac{p_{ej,el}}{kT} = \frac{(\text{charge density})^2}{4e^2N_A I_o} = \frac{x^2\rho_{ej}^2}{4N_A I_o}. \quad (12)$$

The electrostatic pressure is three dimensional, like the membrane–membrane pressure, $p_{j,mm}$, within the junction. Again proceeding as for Eq. 6, we find the lateral pressure

$$\frac{\Pi_{ej,el}}{kT} = \frac{x^2\rho_{ej}^2}{4N_A I_o}2d_{ej}. \quad (13)$$

(C) Conformational Deformation: $\Pi_{ej,cd}$. Compression of the glycocalyx perturbs the conformation of the polymers, with thermodynamic consequences that can be modeled in a variety of ways; Napper (1977) reviews one approach fundamentally related to the Flory–Krigbaum treatment of mixing. For completeness we formally include an elastic contribution to the lateral pressure within our model, although sample calculations (not shown) reveal that such a term is small relative to the electrostatic and mixing terms computed above.

5.3. Results of Modeling

We have analyzed important contributions to the total lateral pressure generated within the gap junction and surrounding glycocalyx. Neglecting boundary effects as discussed, these pressures may be equated at equilibrium, giving

$$\Pi_{j,dd} + \Pi_{j,mm} = \Pi_{ej,el} + \Pi_{ej,mx} + \Pi_{ej,cd}. \tag{14}$$

The quantities $\Pi_{j,mm}$ and $\Pi_{ej,cd}$ were argued equal to zero. The pressure balance equation then contains one free parameter: ρ_{ej}, the number density of polymer segments within the glycocalyx. To test the plausibility of our model, we solve this equation for ρ_{ej} and compare the value obtained with available experimental data.

The solution for ρ_{ej} can be found analytically:

$$\rho_{ej} = \left\{ \frac{\Pi_{j,dd}}{2d_{ej}\left[\frac{x^2}{4N_A I_o} + \frac{V_s^2}{V_l}(1/2 - \chi)\right]} \right\}^{1/2}. \tag{15}$$

The sum in the denominator contains terms from electrostatic and mixing effects. These are approximately equal if all the segments carry charges, that is $x \approx 1$. However, in vivo values of x are closer to one-third to one-fifth (Levine et al., 1983), which after squaring leaves mixing as the predominant component of the extra-junctional lateral pressure.

Parameter values came from a variety of sources. For the electrostatic term, we have chosen $x = 0.33$ (see above), corresponding to one-third of the residues bearing charge, and $N_A I_o = 1.87 \times 10^{20}$ cm^{-3}, where we have approximated the ionic strength of mouse serum by its osmolarity. Values for the mixing term were taken from Bell et al. (1984): $V_s = 3 \times 10^{-22}$ cm^3, the volume of a sugar residue, $V_l = 3 \times 10^{-23}$ cm^3, the volume of a water molecule, and $\chi = 0$, to say that water is a moderately good solvent for sugar. Finally, we have used $d_{ej} = 1.0 \times 10^{-8}$ cm, the thickness of the glycocalyx in an "average cell" (Bongrand et al., 1982).

For the data from junction 1, this choice of parameters gives $\rho_{ej}^{(1)} = 6.0\ (\pm 1.5) \times 10^{19}$/cm^3. The uncertainty was obtained by assuming the various constants were known exactly, with the only variability arising in the dyad–dyad pressure. The same relative error, ±26%, also pertains to the quantities that follow. This sugar density corresponds to a concentration of 99 mM, and a volume fraction of 0.018. The lateral density is obtained via multiplication by d_{ej}, giving $\rho_{ej,lat}^{(1)} = 6.0 \times 10^{13}$/cm^2. The charge concentration is 33 mM, and the lateral charge density is 2.0×10^{13}/cm^2. These relatively low values for the charge density suggest why the electrostatic term is not dominant.

The data for junction 2 give $\rho_{ej}^{(2)} = 4.5\ (\pm 0.8) \times 10^{19}$/cm^3; the lateral density is $\rho_{ej,lat}^{(2)} = 4.5 \times 10^{13}$/cm^2. Other quantities are scaled appropriately from the results presented for junction 1, with a relative error of ±17%.

We chose a maximal weighting for the electrostatic term (on the range presented by Levine et al., 1983). Smaller values of x decrease the importance of the electrostatic term and (minimally) increase the density of sugar residues necessary to get pressure balance. For example, a value of $x = 0.2$ gives $\rho_{ej}^{(1)} = 6.1 \times 10^{19}$/cm^3 and $\rho_{ej}^{(2)} = 4.7 \times 10^{19}$/cm^3.

Similarly, we chose a maximal value for the thickness of the glycocalyx. Smaller values imply an increased residue density. A value of $d_{ej} = 0.75 \times 10^{-6}$ (as in Levine et al., 1983), together with $x = 0.33$, gives $\rho_{ej}^{(1)} = 6.9 \times 10^{19}$/cm^3 and $\rho_{ej}^{(2)} = 5.2 \times 10^{19}$/cm^3.

The terms we have omitted from our calculation both act to decrease slightly the required carbohydrate density within the glycocalyx. Junctional membrane–membrane repulsions act to diminish the size of the junction, thus minimizing the area involved in unfavorable interactions. This requires a smaller value of ρ_{ej} to balance a smaller junctional pressure. Conformation deformation within the glycocalyx acts to expand the glycocalyx to decrease the compression. This also implies a smaller carbohydrate density.

Interpenetration of the cell coat has been considered in detail (Meier, 1967; Smitham et al., 1975; Napper, 1977; Bongrand and Bell, 1983). Interactions with sugars from the neighboring cell strengthen the mixing term and slightly reduce the carbohydrate density necessary to achieve pressure balance.

To summarize our results, while not discounting possible biological variability, we predict a value of ρ_{ej} near 5×10^{19}/cm^3 and a value of $\rho_{ej,lat}$ of 5×10^{13}/cm^2. This result is not overly sensitive to the choices of values for the parameters.

5.4 Discussion of Modeling

To determine the success of our modeling, we compare the results we have derived with those known experimentally. We are unaware of any definitive values for mouse liver cells and so rely, as we did for parameter values, on results from several sources. Bongrand et al. (1982) report a sugar density of $\rho_{ej,lat} = 14 \times 10^{13}$/cm^2 for an "average cell" but based largely on results from erythrocyte membranes. A more refined calculation by Levine et al. (1983) gives a value for the same system of 12×10^{13}/cm^2. Bell et al. (1984) use a value of 5×10^{13}/cm^2 for their calculation of a Flory–Krigbaum term similar to that used in our model.

Results derived from electrophoretic methods on a variety of systems average two to three times smaller than our values (Sherbet, 1978). However, this technique is known to underestimate surface charge by about this amount (Levine et al., 1983), leaving the values in much closer accordance. The general agreement between these values and ours demonstrates adequately that our approach is reasonable. Given the paucity of experimental data, no more definitive test is warranted at this time.

Although presented as an equilibrium model, our work has some implications for dynamic processes involving gap junctions. It is consistent with the consensus view (discusssed in the Introduction) that junctional plaques grow by accretion of freely diffusing monomeric or oligomeric dyads. The model's connection to junctional disassembly is more problematic.

Two modes of disassembly have been proposed: internalization of the plaque (e.g., Ginzberg and Gilula, 1979; Larsen et al., 1981) and the lateral dispersal of the connexons as monomers (e.g., Lane and Swales, 1980; Preus et al., 1981). The cytoskeletal interactions necessary for internalization are not part of the model, but they do not contradict it so long as they operate only during junctional reorganization and not in stable junctions. Dispersal of connexons when dyads are split, and the apposed cell membranes are allowed to separate, is a likely consequence of the model. The splitting of the junction would remove the confining extra-junctional pressure, permitting the connexons to separate under the influence of diffusion and intermolecular repulsions.

It is possible to split most of the gap junctions in the liver by perfusion with hypertonic sucrose solution for 10–30 s, followed by fixation with glutaraldehyde (Goodenough and Gilula, 1974). Examination of such specimens with freeze-fracture electron microscopy reveals junctional plaques that persist with perfusion times at least as long as 2 min (Goodenough and Gilula, 1974; Hirokawa and Heuser, 1982). Plaque borders are smooth, similar to those in intact junctions. At least in some cases these probably represent split junctions, not residual intact junctions.

If the lateral diffusion of the connexons in the split junction is comparable to that of typical membrane proteins, say 10^{-9}–10^{-10} cm^2s^{-1} (McCloskey and Poo, 1984), this persistence seems long: a rough characteristic time for dispersion must be the ratio of the junctional area to the diffusion coefficient, or 10–100 s. There are, however, complications to this simple calculation. First, the connexons in a split junction are in a different conformational state from the dyads that we have analyzed. Being half dyads in the closed state, they may interact by forces that differ considerably from those we have observed. Attractions that retard dispersion cannot be ruled out at this time. Second, it is not at all well understood quantitatively how protein–protein interactions affect lateral diffusion, particularly in a dense plaque. We are developing a theoretical approach to the subject (Abney et al., 1987), and direct experimental measurements of lateral mobility in junctional plaques would be very useful. Finally, there may exist more than one population of junctions (Goodenough and Gilula, 1974). These could include junctions in the process of internalization or reorganization, where factors we have not considered could play a role in maintaining junctional cohesiveness. Experiments such as those described here would reveal only those junctions that did not disperse.

6. SUMMARY AND CONCLUSIONS

We have shown that the short-range order of proteins within mouse liver gap junctions is characteristic of interacting particles in a fluid state. With this in mind, we have applied a fluid-theoretic approach to extract the forces acting among these proteins from high-quality freeze-fracture electron micrographs, without strong restrictive assumptions about the functional form of the forces. The forces thus found were qualitatively interpreted to arise from electrostatic and excluded volume interactions.

We have also shown that knowledge of interprotein interactions can lead to useful insights into the organization of cell membranes. This is true even though the detailed physical origins of the interactions are not completely clear. We have proposed a quantitative model for the mechanisms that maintain the aggregated state of gap junctions in the face of the repulsions between dyads that we have computed. We believe that forces acting to compress the gap junction laterally arise in the extra-junctional glycocalyx, and indirectly but ultimately result from the close apposition of membranes in the junctional region.

Our model differs from the one presented with preliminary results (Braun et al., 1984) in its emphasis on the glycocalyx as the proximate compressive factor. This emphasis is taken from a very similar but qualitative model proposed independently by Peracchia (1985). A kinetic model, primarily to explain the formation of junctional plaques rather than their maintenance, was presented by Loewenstein (1981). In it, diffusing hemi-channels are trapped in junctional regions of close membrane apposition when they pair up to form dyads. Their diffusion away from the junction is opposed by the bending movement of the membranes at the edge of the plaque. This model has some features in common with ours but does not incorporate most of the forces that we have discussed.

Finally, we note that our model has wider applications than to gap junctions. Regions of close apposition between cells occur in developmental and immunological contexts, and many features of our system should appear there. Our treatment of the glycocalyx was, in fact, inspired in part by the work of Bell and colleagues (e.g., Bell et al., 1984) on the more general case of cell adhesion.

We are pleased to acknowledge Elio Raviola's generosity in supplying the micrographs without which this paper could not have been written.

Computer access for some of the work was kindly provided by Donald Glaser and Robert Henry. We thank Aaron Kantor, Bethe Scalettar, Sid Simon, and Nigel Unwin for helpful conversations. Aaron Kantor and Bethe Scalettar also provided invaluable comments on the manuscript.

This work received support from National Institute of Health (NIH) grants AI19605 and AI22860, and a grant from the U. C. Cancer Research Coordinating Committee. J. R. Abney was an NIH trainee (grant GM07379), and J. Braun was supported in part by the German National Fellowship Foundation.

Received for publication 17 December 1986 and in final form 5 May 1987.

REFERENCES

Abney, J. R., and J. C. Owicki. 1985. Theories of protein-lipid and protein-protein interactions in membranes. *In* Progress in Protein-Lipid Interactions. A. Watts and J.J.H.H.M. de Pont, editors. Elsevier Science Publishers, Amsterdam. 1–59.

Abney, J. R., B. A. Scalettar, and J. C. Owicki. 1987. Concentration and time dependent self-diffusion of interacting membrane proteins. *Biophys. J.* 51:541a. (Abstr.)

Adamson, A. W. 1982. Physical Chemistry of Surfaces. John Wiley & Sons, Inc., New York.

Bell, G. I., M. Dembo, and P. Bongrand. 1984. Cell adhesion: competition between nonspecific repulsion and specific bonding. *Biophys. J.* 45:1051–1064.

Bennett, M. V. L., and D. C. Spray. 1985. Gap Junctions. Cold Spring Harbor Laboratory, Cold Spring Harbor, NY.

Bevington, P. R. 1969. Data Reduction and Error Analysis for the Physical Sciences. McGraw-Hill Book Co., New York.

Bongrand, P., and G. I. Bell. 1983. Cell-cell adhesion: parameters and possible mechanisms. *In* Cell Surface Dynamics: Concepts and Models. C. DeLisi, A. Perelson, and F. Wiegel, editors. Marcell Dekker, New York. 459–493.

Bongrand, P., C. Capo, and R. Depieds. 1982. Physics of cell adhesion. *Prog. Surf. Sci.* 12:217–285.

Braun, J., J. R. Abney, and J. C. Owicki. 1984. How a gap junction maintains its structure. *Nature (Lond.).* 310:316–318.

Braun, J., J. R. Abney, and J. C. Owicki. 1987. Lateral interactions among membrane proteins: valid estimates based on freeze-fracture electron microscopy. *Biophys. J.* 52:427–439.

Caspar, D. L. D., D. A. Goodenough, L. Makowski, and W. C. Phillips. 1977. Gap junction structures: I. Correlated electron microscopy and x-ray diffraction. *J. Cell Biol.* 74:605–628.

Croxton, C. A. 1980. Statistical Mechanics of the Liquid Surface. John Wiley & Sons, Inc., New York.

DeMello, W. C. 1984. Cell-to-cell communication. Introductory remarks. *Fed Proc.* 43:2671.

Flory, P. J., and W. R. Krigbaum. 1950. Statistical mechanics of dilute polymer solutions. II. *J. Chem. Phys.* 18:1086–1094.

Gilula, N. B. 1974. Junctions between cells. *In* Cell Communication. R. S. Cox, editor. John Wiley & Sons, Inc., New York. 1–29.

Ginzberg, R. D., and N. B. Gilula. 1979. Modulation of cell junctions during differentiation of the chicken otocyst sensory epithelium. *Dev. Biol.* 68:110–129.

Goodenough, D. A., and N. B. Gilula. 1974. The splitting of hepatocytic gap junctions and zonulae occludentes with hypertonic disaccharides. *J. Cell Biol.* 61:575–590.

Green, C. R., and N. J. Severs. 1984. Connexon rearrangement in cardiac gap junctions: evidence for cytoskeletal control? *Cell Tissue Res.* 237:185–186.

Gros, D., B. Bruce, C. E. Challice, and J. Schrevel. 1982. Ultrastructural localization of Concanavalin A and wheat germ agglutinin binding sites in adult and embryonic mouse myocardium. *J. Histochem. Cytochem.* 30:193–200.

Gumbiner, B., and D. Louvard. 1985. Localized barriers in the plasma membrane: a common way to form domains. *Trends Biochem. Sci.* 10:435–438.

Hertzberg, E. L., and N. B. Gilula. 1979. Isolation and characterization of gap junctions from rat liver. *J. Biol. Chem.* 254:2138–2147.

Heuser, J. E., T. S. Reese, M. J. Dennis, Y. Jan, L. Jan, and L. Evans. 1979. Synaptic vesicle exocytosis captured by quick freezing and correlated with quantal transmitter release. *J. Cell Biol.* 81:275–300.

Hill, T. 1956. Fundamental studies on the theory of the Donnan membrane equilibrium. *Faraday Soc. Disc.* 21:31–45.

Hill, T. 1960. Statistical Thermodynamics. Addison-Wesley Publishing Co. Inc., Reading, MA.

Hirokawa, N., and J. Heuser. 1982. The inside and outside of gap-junction membranes visualized by deep etching. *Cell.* 30:395–406.

Ito, S., E. Sato, and W. R. Loewenstein. 1974. Studies on the formation of a permeable cell membrane junction. *J. Membr. Biol.* 19:305–337.

Johnson, R., M. Hammer, J. Sheridan, and J.-P. Revel. 1974. Gap junction formation between reaggregated Novikoff hepatoma cells. *Proc. Natl. Acad. Sci. USA.* 71:4536–4540.

Lane, N. J., and L. S. Swales. 1980. Dispersal of junctional particles, not internalization, during the in vivo disappearance of gap junctions. *Cell.* 19:579–586.

Larsen, W. J. 1983. Biological implications of gap junction structure, distribution and composition: a review. *Tissue & Cell.* 15:645–671.

Larsen, W. J., H. N. Tung, and C. Polking. 1981. Response of granulosa cell gap junctions to human chorionic gonadotropin (hCG) at ovulation. *Biol. Reprod.* 25:1119–1134.

Levine, S., M. Levine, K. A. Sharp, and D. E. Brooks. 1983. Theory of the electrokinetic behavior of human erythrocytes. *Biophys. J.* 42:127–135.

Lewis, G. N., and M. Randall. 1961. Thermodynamics. McGraw-Hill Book Co., New York.

Loewenstein, W. R. 1981. Junctional intercellular communication. The cell-to-cell membrane channel. *Physiol. Rev.* 61:829–913.

Makowski, L., D. L. D. Caspar, W. C. Phillips, and D. A. Goodenough. 1977. Gap junction structures: II. Analysis of the x-ray diffraction data. *J. Cell Biol.* 74:629-645.

McCloskey, M., and M.-m. Poo. 1984. Protein diffusion in cell membranes: Some biological implications. *Int. Rev. Cytol.* 87:19–81.

McQuarrie, D. A. 1976. Statistical Mechanics. Harper and Row, New York.

Meier, D. J. 1967. Theory of polymeric dispersants. Statistics of constrained polymer chains. *J. Phys. Chem.* 71:1861–1868.

Metropolis, N., A. Rosenbluth, M. Rosenbluth, A. Teller, and E. Teller. 1953. Equations of state calculations by fast computing machines. *J. Chem. Phys.* 27:720–733.

Napper, D. H. 1977. Steric stabilization. *J. Colloid Interface Sci.* 58:390–407.

Pearson, L. T., J. Edelman, and S. I. Chan. 1984. Statistical mechanics of lipid membrane: protein correlation functions and lipid ordering. *Biophys. J.* 45:863–871.

Peracchia, C. 1985. Cell coupling. *In* The Enzymes of Biological Membranes. Vol 1. A. Martonosi, editor. Plenum Publishing Corp., New York. 81–160.

Peracchia, C., and L. L. Peracchia. 1980. Gap junction dynamics: reversible effects of divalent cations. *J. Cell Biol.* 87:708–718.

Peracchia, C., and L. L. Peracchia. 1985. Bridges linking gap junction particles extracellularly: a freeze-etching rotary-shadowing study of split junctions. *Eur. J. Cell Biol.* 36:286–293.

Preus, D., R. Johnson, and J. Sheridan. 1981. Gap junctions between Novikoff hepatoma cells following dissociation and recovery in the absence of cell contact. *J. Ultrastruct. Res.* 77:248–262.

Rand, R. P., and V. A. Parsegian. 1984. Physical force considerations in model and biological membranes. *Can. J. Biochem. Cell Biol.* 62:752–759.

Rassat, J., H. Robenek, and H. Themann. 1981. Ultrastructural alterations in the mouse liver following vincristine administration. *J. Submicrosc. Cytol.* 13:321–335.

Rassat, J., H. Robenek, and H. Themann. 1982. Alterations of tight and gap junctions in mouse hepatocytes following administration of colchicine. *Cell Tissue Res.* 223:187–200.

Raviola, E., D. A. Goodenough, and G. J. Raviola. 1980. Structure of rapidly frozen gap junctions. *J. Cell Biol.* 87:273–279.

Ryerse, J. S., B. A. Nagel, and I. Hammel. 1984. The role of connexon aggregate fusion in gap junction growth. *J. Submicrosc. Cytol.* 16:649–657.

Savitzky, A., and M. J. E. Golay. 1964. Smoothing and differention of data by simplified least squares procedures. *Anal. Chem.* 36:1627–1639.

Sherbet, G. V. 1978. The Biophysical Characterization of the Cell Surface. Academic Press, London.

Shivers, R. R., and P. D. Bowman. 1985. A freeze-fracture paradigm of the mechanism for delivery and insertion of gap junction particles into the plasma membrane. *J. Submicrosc. Cytol.* 17:199–203.

Smitham, J. B., R. Evans, and D. H. Napper. 1975. Analytical theories of the steric stabilization of colloidal dispersions. *J. Chem. Soc. Faraday Trans. I.* 71:285–297.

Tadvalkar, G., and P. Pinto da Silva. 1983. In vitro, rapid assembly of gap junctions is induced by cytoskeleton disruptors. *J. Cell Biol.* 96:1279–1287.

Tsien, R. Y. 1978 A virial expansion for discrete charges buried in a membrane. *Biophys. J.* 24:561–567.

Tsien, R. Y., and S. B. Hladky. 1982. Ion repulsion within membranes. *Biophys. J.* 39:49–56.

Unwin, P. N. T., and G. Zampighi. 1980. Structure of the junction between communicating cells. *Nature (Lond.).* 283:545–549.

Wrigley, N. G., E. Brown, and R. K. Chillingworth. 1984. Reversible structure transition in gap junction under Ca^{++} control seen by high-resolution electron microscopy. *Biophys. J.* 45:201–207.

Yee, A. G., and J.-P. Revel. 1978. Loss and reappearance of gap junctions in regenerating liver. *J. Cell Biol.* 78:554–564.

Zampighi, G. A., and S. A. Simon. 1985. The structure of gap junctions as revealed by electron microscopy. *In* Gap Junctions. M. V. L. Bennett and D. C. Spray, editors. Cold Spring Harbor Laboratory. Cold Spring Harbor, NY. 13–22.